Use of low-field NMR and rheology to evaluate the microstructure and stability of a poly(D,L-lactide-*co*-glycolide)-based W/O emulsion to be processed by spray drying

Ana Jurić Simčić [a], Michela Abrami [b], Iva Erak [a], Iva Paladin [a], Biserka Cetina Čižmek [a], Anita Hafner [c], Mario Grassi [b,*], Jelena Filipović-Grčić [c,*]

[a] *R&D, PLIVA Croatia Ltd, TEVA Group Member, Prilaz baruna Filipovića 25, 10000 Zagreb, Croatia*
[b] *Department of Engineering and Architecture, Trieste University, via Valerio 6, I-34127 Trieste, Italy*
[c] *University of Zagreb, Faculty of Pharmacy and Biochemistry, A. Kovačića 1, 10000 Zagreb, Croatia*

ARTICLE INFO

Keywords:
W/O emulsion
Poly(D,L-lactide-*co*-glycolide) (PLGA)
Vancomycin hydrochloride
Spray drying
Low-field NMR
Rheology

ABSTRACT

Drug-loaded emulsions for spray drying should be optimised for their rheological behaviour and stability under operating conditions, as this is essential for achieving the desired physicochemical properties of the final dry product. Our aim was therefore to investigate the structure and stability of a water-in-oil (W/O) emulsion containing vancomycin hydrochloride as the active ingredient in the aqueous phase, poly(D,L-lactide-*co*-glycolide) as the structural polymer in the dichloromethane-based organic phase, and various stabilisers using low-field nuclear magnetic resonance (LF NMR) and rheological characterisation. Four emulsions were tested, namely-one without stabiliser, one with Poloxamer® 407, one with chitosan and Span™ 80 and one with chitosan only. The theoretical interpretation of the rheological data allowed the determination of the velocity and the shear rate/stress profiles inside the feed path of the W/O emulsion, aspects that are critical for the industrial scale-up of the emulsion drying process. In addition, LF NMR demonstrated that shaking was sufficient to restore the original emulsion structure and that the droplet size of all emulsions was in the range of 1–10 μm, although the emulsion with chitosan had the narrowest droplet size distribution and the higher zero shear viscosity, which accounts for the increased long-term stability due to impeded droplets movement.

1. Introduction

In industrial production, parenteral microparticles are manufactured in an aseptic process to ensure the sterility of the final product. Polymeric microparticles containing hydrophilic drugs can be prepared by spray drying, as an alternative to a complex, multi-step double emulsion method (Liu et al., 2010). Spray drying is a fast, scalable technology and a continuous process for the preparation of drug-loaded polymeric microparticles with good control of physicochemical properties. First, the measured amount of water-soluble drug is dissolved in the aqueous phase and the polymer in a suitable organic solvent. Then the aqueous drug phase is added to the organic polymer phase with vigorous stirring to obtain a W/O emulsion. The primary emulsion is generally prepared under high shear forces to produce stable, fine droplets of W/O emulsion. The emulsion is being pumped and atomized into droplets inside a chamber filled with heated gas to evaporate the solvent and form a dry powder product (Ye et al, 2010; Wan and Yang, 2016).

The W/O emulsion is an intermediate product whose stability during the spray drying process is critical to achieve the desired physicochemical properties of the final dry product. The feed emulsion is mixed and pumped during its transport to the atomising nozzle, which allows the droplets of the dispersed phase to deform. Droplet deformation and break-up is a key mechanism in the flow-induced evolution of the microstructure of two-phase liquid–liquid systems such as emulsions (Guido, 2011). The deformation of the droplets and the mechanisms of break-up depend on the viscosity of both the dispersed and continuous phases of the emulsion, the surface tension at the interface of the two liquids and the nature of the flow. The spherical emulsion droplets are

* Corresponding authors.
E-mail addresses: Ana.Juric.Simcic@pliva.com (A. Jurić Simčić), michela.abrami@dia.units.it (M. Abrami), Iva.Erak@pliva.com (I. Erak), Iva.Paladin@pliva.com (I. Paladin), Biserka.Cetina-Cizmek@pliva.com (B. Cetina Čižmek), ahafner@pharma.unizg.hr (A. Hafner), mario.grassi@dia.units.it (M. Grassi), jfilipov@pharma.unizg.hr (J. Filipović-Grčić).

deformed into ellipsoids aligned along the direction of the shear forces. The axial ratio of the droplets increases with shear rate and droplet volume and decreases with increasing interfacial tension. The viscosity ratio between the dispersed and continuous phases is important for the deformation of the dispersed droplets in a two-phase fluid system. Under experimental conditions, the maximum deformation is observed when the viscosity ratio is about one (Tolstoguzov et al., 1974; Janssen and Meijer, 1993). The rheology of the feed fluid is one of the key properties affecting spray performance and has a direct influence on the droplet size distribution produced by atomizing nozzle (Porfirio et al., 2021). The study of droplet flow behaviour is more complicated in concentrated systems due to the hydrodynamic interactions between droplets and complex flow geometries. In fact, the rheological properties of these materials are linked by a complex interplay with the flow conditions, as a flow-induced change in microstructure can in turn affect the system viscosity (Guido and Preziosi, 2010).

During emulsification, drug molecules are exposed to mechanical shear forces and can be adsorbed at the interface between the aqueous and organic phases, which may adversely affect their stability and pharmacological activity, especially for macromolecules and antibiotics (Kang et al., 2002; Shah et al., 2014). Formulation additives such as lipophilic surfactants, amphiphilic surfactants and viscosity enhancing agents can improve the stability of a W/O emulsion, and protect the drug molecule from deformation and denaturation at the interface (Taghipour et al., 2014). They act through electrostatic or steric effects on the dispersed droplets and reduce the occurrence of emulsion instability due to coalescence, flocculation or Ostwald ripening (Panigrahi et al., 2021). Incorporation of a hydrophilic polymer, such as chitosan, into the dispersed aqueous phase of the emulsion has been suggested as a way to improve the long-term stability of W/O emulsions, especially when the added polymer forms a network throughout the inner water droplet or a gel-like layer at the inner oil–water interface (McClements and Dickinson, 1996; Zhu et al., 2019). However, increased viscosity can hinder droplet formation, and lead to the formation of larger emulsion droplets, provided that all other parameters (stirring energy, viscosity of the outer phase) are kept constant (Mohammed et al., 2016). Furthermore, due to its polycationic structure, chitosan plays an important role in improving stability through electrostatic stabilisation (Klinkesorn, 2013). Poloxamers are polymeric and amphiphilic molecules that adsorb at the oil–water interface and form layers around emulsion droplets, making them efficient emulsifiers and stabilizers (Zhang et al., 2017). Sorbitan esters are low HLB lipophilic surfactants, commonly used as stabilizers for PLGA-based W/O emulsions (Billon et al., 2005; Soomherun et al., 2017; Dinarvand et al., 2005, Panigrahi et al., 2021).

The aim of this work is to investigate the influence of formulation additives on the stability, droplet size and rheology of a W/O emulsion containing vancomycin hydrochloride and PLGA. It contributes to the rheological characterisation of a PLGA/DCM-based emulsion, which is very limited in the literature. A theoretical approach was used to describe the flow conditions in the tube and the emulsion feed path in the spray drying process.

To the best of our knowledge, this is the first study to consider the synergy of rheology and low-field NMR to investigate some important structural features of a PLGA-based W/O emulsion, e.g. the droplet size distribution, the volume fraction of the different phases present in the emulsion and the corresponding relaxation time which, together, form the magnetic fingerprint of the emulsion. This, in turn, is closely linked to the emulsion structure. In addition, the combination of low-field NMR and rheology can provide information that a single technique cannot, such as the fact that while all emulsions have similar droplet sizes, the differences between their flow curves are due to the different viscosity behaviour of the organic and aqueous phases that make up each emulsion.

2. Materials and methods

2.1. Materials

Vancomycin hydrochloride was purchased from Guangzhou Greensyn Pharma Co., ltd. (Guangzhou, China). Evonik (Darmstadt, Germany) was the supplier of poly(D,L-lactide-*co*-glycolide) (Resomer® RG 502H, L/G ratio 50/50, acid terminated, M_w 7,000–17,000 Da, inherent viscosity 0.16–0.24 dl/g in chloroform at 25 °C). Chitosan (from shrimp shells, low viscosity (20 – 200 mPas, c = 1 wt% in 1 % acetic acid)) was purchased from Sigma-Aldrich (Steinheim, Germany). Poloxamer 407 (P407), a poly(ethylene oxide)-poly(propylene oxide)-poly(ethylene oxide) (PEO-PPO-PEO) triblock copolymer, was purchased from BASF (Ludwigshafen, Germany). Sorbitan monooleate (Span™ 80) was purchased from Croda (Barcelona, Spain). Dichloromethane was purchased from Merck (Darmstadt, Germany). Other materials were of analytical grade.

2.2. Preparation of W/O emulsions

Four emulsion formulations containing vancomycin hydrochloride in the aqueous phase and PLGA in the organic phase were prepared. The dispersed aqueous phase (5 g) of all emulsion formulations was prepared by dissolving vancomycin hydrochloride (625 mg) in purified water. To obtain the continuous organic phase (50 g), PLGA (2.5 g) was dissolved in dichloromethane. In emulsion F2, P407 (50 mg) was dissolved with vancomycin hydrochloride in the aqueous phase. In emulsion F4, chitosan (50 mg) was dissolved in the aqueous phase with vancomycin hydrochloride, while emulsion F3 contained chitosan (50 mg) in the aqueous phase and sorbitan monooleate (100 mg) in the organic phase.

The emulsions were prepared by ultrasonication using Sonopuls HD 4200 with titanium flat tip TT213 (BANDELIN electronic GmbH & Co. KG, Berlin, Germany), 30 s at 100 % amplitude in a cold bath. The composition of the prepared emulsions is shown in Table 1. In order to investigate the stabilising effect of formulation additives, the corresponding empty emulsions (FB1 – FB4, without vancomycin hydrochloride in the dispersed phase) were also prepared.

2.3. Characterisation of the W/O emulsions

2.3.1. Visual inspection

Immediately after their preparation, the emulsions were viewed microscopically with Olympus BX51 light microscope (Olympus, Japan) at 50x magnification and stored in well-sealed glass vials at room temperature for 24 h. During this time, emulsions were visually monitored for signs of phase separation. After 24 h of ageing at a room temperature, samples were redispersed by shaking and examined microscopically again.

2.3.2. DLS

Dynamic Light Scattering (DLS) measurements were conducted on Zetasizer Ultra instrument from Malvern Panalytical (Worcestershire, UK). Quartz cuvette ZEN2112 was used for holding the sample. The emulsions F1-F4 were analyzed upon preparation and after 24 h storage

Table 1
Composition of the W/O emulsions.

Formulation	Aqueous phase (% w/w), 5 g			Organic (DCM) phase (% w/w), 50 g	
	Vancomycin hydrochloride	P407	Chitosan	PLGA	Sorbitan monooleate
F1	12.5	–	–	5	–
F2	12.5	1	–	5	–
F3	12.5	–	1	5	0.2
F4	12.5	–	1	5	–

at room temperature. The analyses were done in triplicate at a temperature of 25 °C. Scattering collection angle was 174,7°.

2.3.3. Low-field nuclear magnetic resonance (LF NMR)

LF NMR measurements were performed with a Bruker Minispec mq20 (0.47 T, Karlsruhe, Germany).

2.3.3.1. Relaxation time. Determination of the average spin–spin relaxation time (T_{2m}) of the hydrogens present in freshly prepared and 24 h aged emulsions was performed according to the CPMG sequence (Meiboom and Gill, 1958) {90°[-τ-180°-τ(echo)]$_n$-T_R} with a 8.36 μs wide 90°pulse, τ = 250 μs, and T_R (sequences repetition rate) equal to 10 s.

The initial amplitude of the decay curve ($I(t)$) is directly proportional to the number of polarized hydrogen dipoles in the fluid and can be properly fit by a sum of decaying exponentials, each one characterized by a different transverse relaxation time T_{2i} (Chui and Phillips, 1995):

$$I(t) = \sum_{i=1}^{m} A_i exp(-t/T_{2i}) \tag{1}$$

where t is time. The set of all the decay constants T_{2i} and their relative abundance A_i represents the decay spectrum or the transverse-relaxation-time distribution (A_i -T_{2i}). This simply means that the faction A_i of all the dipoles relaxes with the time constant T_{2i}. Consequently, it is possible to define an average relaxation time T_{2m}:

$$T_{2m} = \sum_{i=1}^{m} A_i T_{2i} \Big/ \sum_{i=1}^{m} A_i \qquad A_{i\%} = 100A_i \Big/ \sum_{i=1}^{m} A_i \tag{2}$$

The number, m, of the relaxation times (T_{2i}) constituting the relaxation time distribution was determined by minimizing the product $\chi^2 \times (2m)$, where χ^2 is the sum of the squared errors and $2m$ represent the number of fitting parameters in eq. (1) (i.e. the "m" A_i and the "m" T_{2i}) (Draper and Smith, 1966).

2.3.3.2. Droplet size distribution. Droplet size distribution of the dispersed phase was determined from the relaxation time (T_2) of the two liquid phases and the self-diffusion coefficient (D) of the dispersed phase molecules. The sequence used is the CPMG sequence described earlier, to which two magnetic field gradients have been added, one after the 90° pulse (the first one) and the other after the 180° pulse (the second one). The second gradient, acting in the opposite way with respect to the first one, occurs after a time interval Δ from the first one, while the equal duration of each gradient is called δ. Varying both time intervals Δ and δ, it is possible measuring the self-diffusion coefficient of the dispersed liquid phase molecules. Indeed, if the liquid molecules were fixed in the space, the second gradient would perfectly restore the situation perturbed by the first one. Thus, signal intensity $I(t)$ would be the same with or without gradients application. If, on the contrary, liquid molecules move (diffuse), the second gradient cannot restore the perturbation caused by the first one so that signal intensity $IG(t)$ would be lower than signal intensity without gradients application $I(t)$. Thus, it can be argued that the IG/I ratio (R) is connected to the liquid self-diffusion coefficient. This connection is given by a well known equation (Stilbs, 1987).

The idea is that the diffusion of the dispersed liquid molecules is limited (restricted diffusion) by droplets diameter d since they cannot go inside the continuous liquid phase due to liquids immiscibility. Thus, it is necessary setting a value of Δ (Δ_{min}) such that the ratio R remains constant for bigger Δ and different δ values. We can say that the "fingerprint" of the emulsion is given by the R dependence on δ, being Δ = Δ_{min}. In so doing, we also guarantee that the relaxation of the dispersed phase (characterized by a smaller T_2) has come to completion. Consequently, we are studying the relaxation of the continuous phase (characterized by the higher T_2). This means that the greater the difference between the relaxation time of the continuous phase and the dispersed phase, the more reliable the droplet size distribution (in this case, the manufacturer recommends performing the measurements at 20 °C). This situation usually occurs with microemulsions of oil (low relaxation time) in water (high relaxation time). In our case, however, the aqueous phase is characterised by a lower relaxation time than the oil phase because it contains solids (such as polymers) that greatly reduce the relaxation time. Therefore, we treated the aqueous phase like an ordinary oil phase and vice versa. As R depends on Δ_{min}, δ, D, gradient strength g and droplets size distribution, by fitting the experimental R data vs δ (being all other parameters constant) with a proper, complex, mathematical model relaying on the hypothesis that droplet size distribution can be properly described by a log-Normal distribution (MQ20 Bruker Manual), it is possible getting the droplets size distribution:

$$f(d) = \frac{e^{\left(-\frac{(\ln(d)-\ln(d_{50}))^2}{2\sigma^2}\right)}}{\sigma d\sqrt{2\pi}} \tag{3}$$

where f is frequency, d is droplets diameter, σ is the dimensionless distribution standard deviation and d_{50} represents the geometric mean diameter (50 % of droplets are smaller and 50 % larger than this diameter). The low-field NMR instrument provides as output σ and d_{50} for both the number ($d_{50\text{-}0}$) and the volume ($d_{50\text{-}3}$) distribution. Notably, σ is the same for the number and the volume distributions.

2.3.4. Rheology

At rest phase, the emulsion droplets have the shape of spheres. When they flow, their size and shape change into an ellipsoid, according to shear. Since the droplets then have a smaller cross-section in the direction of flow, the viscosity of emulsion decreases, which is described as the shear-thinning flow behaviour (Mezger, 2015). In order to theoretically evaluate the shear rate ($\dot{\gamma}$) and the shear stress (τ_{rz}) experienced by the emulsions inside the feed tubing, its flow curve (i.e. the dependence of emulsion shear viscosity (η) vs $\dot{\gamma}$ or τ_{rz}) was determined. At this purpose, a HAAKE Mars III rheometer, equipped by a plate-plate (diameter 60 mm) measure device embedded inside a solvent trap to prevent from evaporation, was used. Measurements were performed at 20 °C according to the temperature fixed for the low-field NMR determination of droplet size distribution.

2.3.4.1. Models for rheological data characterization. Preliminary tests have proven the hypothesis that the emulsions exhibit a non-Newtonian behavior characterized by a viscosity reduction with $\dot{\gamma}$ or τ_{rz} (shear thinning). The classical power law model (eq. (4)) and the Reiner-Philippoff model, generalized in the spirit of the Cross model (R-P Cross eq. (5)), were fitted to the experimental data (η vs $\dot{\gamma}$ and τ_{rz}, respectively):

$$\eta = \eta_0 \dot{\gamma}^{n-1} \qquad \text{power law} \tag{4}$$

$$\eta = \eta_\infty + \frac{\eta_0 - \eta_\infty}{1 + (\tau_{rz}/\tau_s)^{(1-n)}} \qquad \text{R} - \text{P Cross} \tag{5}$$

where η_0 is the shear viscosity at zero shear/stress, η_∞ is the shear viscosity at very high shear/stress, while n and τ_s are two model parameters.

In order to describe the flow conditions experienced by a fluid flowing (according to a laminar flow) inside a round tube, it is necessary solving the momentum balance in stationary conditions considering the proper expression for the shear viscosity dependence on the shear rate/stress. The solution of the momentum balance yields to (Bird et al., 2015):

$$\tau = \frac{r}{2}\left[-\frac{\Delta p}{L} - \rho g sin(\beta)\right] = -\eta\dot{\gamma} \tag{6}$$

where r is the radial coordinate, L is tube length, Δp is the pressure drop across the tube, ρ is fluid density, g is acceleration gravity and β is

tube inclination with respect to a horizontal line (β = 0).

Power Law.

Introducing the power law (eq. (4)) in eq. (6):

$$\tau = \frac{r}{2}\left[-\frac{\Delta p}{L} - \rho g sin(\beta)\right] = -\eta_0 \dot{\gamma}^n \tag{7}$$

Solving for $\dot{\gamma}$ and remembering that $\dot{\gamma} = \frac{dv_z}{dr}$:

$$\dot{\gamma} = \frac{dv_z}{dr} = -\left(\frac{r}{2\eta_0}\left[-\frac{\Delta p}{L} - \rho g sin(\beta)\right]\right)^{\frac{1}{n}} \tag{8}$$

where v_z is the fluid velocity in the direction of the tube axis (z). The solution of eq. (8) under proper boundary condition ($v_z = 0$ on the tube wall $r = R_p$) leads to the velocity profile ($v_z(r)$) and the $\dot{\gamma}(r)$ trend:

$$v_z = v_{zmax}\left[1 - \left(\frac{r}{R_p}\right)^{\frac{n+1}{n}}\right] \qquad v_{zmax} = \left(\frac{1}{2\eta_0}\left[-\frac{\Delta p}{L} - \rho g sin(\beta)\right]\right)^{\frac{1}{n}} R_p^{\frac{n+1}{n}} \frac{n}{n+1} \tag{9}$$

$$\dot{\gamma} = -\frac{n+1}{n}\frac{v_{zmax}}{R_p}\left(\frac{r}{R_p}\right)^{\frac{1}{n}} \tag{10}$$

Remembering that the fluid flow rate Q is given by:

$$Q = \int_0^{R_p} 2\pi r v_z(r) dr \tag{11}$$

The analytical expression for the flow rate is:

$$Q = \pi v_{zmax} R_p^2 \frac{n+1}{3n+1} \tag{12}$$

Generalized Reiner-Philippoff.

Introducing the R-P Cross model (eq.(5)) in eq.(6):

$$\tau = \frac{r}{2}\left[-\frac{\Delta p}{L} - \rho g sin(\beta)\right] = -\left(\eta_\infty + \frac{\eta_0 - \eta_\infty}{1 + (\tau/\tau_s)^{(1-n)}}\right)\dot{\gamma} \tag{13}$$

Thus, it follows:

$$\dot{\gamma} = \frac{dv_z}{dr} = -\frac{\alpha\frac{r}{2}}{\left(\eta_\infty + \frac{\eta_0 - \eta_\infty}{1+\left(\alpha\frac{r}{2}/\tau_s\right)^{(1-n)}}\right)} \qquad \alpha = -\frac{\Delta p}{L} - \rho g sin(\beta) \tag{14}$$

Eq. (14) integration leads to:

$$v_z(r) = \int_r^{R_p} \frac{\alpha\frac{r}{2}\left(1 + (\alpha r/2\tau_s)^{(1-n)}\right)}{\eta_\infty(\alpha r/2\tau_s)^{(1-n)} + \eta_0} dr \tag{15}$$

The numerical solution (trapezoid rule) of eq. (15) allows to get the velocity profile inside the tube once α is properly set to match the desired flow rate Q that is given by eq. (11). Once α is known, eq. (13) and (14) allow, respectively, the determination of the shear stress and the shear rate inside the tube.

3. Results and discussion

3.1. Emulsion appearance and physical stability

Considering the duration of the large scale emulsification/spray drying process and the time constraints of aseptic processing, a period of 24 h was chosen for monitoring emulsion stability. The obtained emulsions F1, F2, F3 and F4 (with the composition described in Table 1) were milky white and homogeneous. Microscopic examination of the freshly prepared emulsions (Fig. 1, left panels) showed only minor differences between the emulsion formulations.

About 2 h after preparation, the emulsions began to separate, which was visually noticeable by a slight discolouration at the bottom of the vial. The emulsions were redispersed by shaking 24 h after preparation and examined again microscopically. The microscopic appearance of the redispersed emulsions was very similar to that immediately after preparation - there was no obvious change in droplet size (Fig. 1, right panels). This suggests that physical segregation of the emulsion phases during storage occurred through the formation of weak, reversible flocs that were easily broken up by shaking, while the droplets of the dispersed phase retained their integrity (Tadros, 2016).

In this work, a low viscosity type of PLGA was used. However, a low molecular weight polymer is less effective in stabilising the emulsion than a higher molecular weight polymer at the same concentration. In general, the presence of a polymer in the continuous phase forms a steric barrier around the dispersed droplets, stopping their movement and reducing contact between the droplets, thus preventing agglomeration (Behrend et al., 2000).

Visual observation of empty emulsions (without the vancomycin hydrochloride dissolved in the dispersed aqueous phase) for 24 h at room temperature helped to clarify the effects of the formulation additives (poloxamer 407, sorbitan monooleate, chitosan) on the stability of the emulsion based on 5 wt% Resomer® RG 502H in DCM. Emulsions containing water (without the solute, blank emulsion FB1) and poloxamer 407 at 1 wt% (blank emulsion FB2) in the aqueous phase undergo complete phase separation within a few hours after preparation. In contrast, when vancomycin hydrochloride is present in the aqueous phase, the emulsions remain stable for 24 h, as observed from Fig. 1 (emulsions F1 and F2). Vancomycin interacts with the polymer chains, probably through ionic interactions, and forms an interfacial film. The chosen PLGA polymer doesn't have capped terminal carboxyl groups that could allow ionic interactions between the carboxyl group of the polymer and the positively charged amino acid groups of the glycopeptide (De Rosa et al., 2000). Therefore, the electrostatic interaction between positively charged groups of the vancomycin and negatively charged PLGA end groups is responsible for the reversible flocculation of the described W/O emulsions.

Empty emulsions containing 1 % chitosan in the aqueous phase (FB3 and FB4) and the corresponding emulsions containing vancomycin hydrochloride dissolved in the aqueous phase (F3 and F4) show a similar visual appearance over a 24-hour period. Since chitosan is also a polycationic compound that can interact with negatively charged surfaces such as the PLGA end groups, this observation suggests that chitosan stabilises the emulsion by electrosteric interaction.

The results deriving from DLS measurements, reported in Table 2, show that the four emulsions do not differ too much from each other for what concerns the mean particles diameter that spans from about 1.6 μm to 2.1 μm. In addition, the mean particle size after 24 h of storage and shaking is very similar for all emulsions considered.

3.2. Low-field NMR determination of relaxation behaviour and size distribution of emulsion droplets

NMR is a non-invasive tool for characterising emulsions and does not require transparency of the system as is the case with optical methods. Moreover, it characterises the entire measurement volume and not only the surface visible with optical methods (Sjöblom et al., 2021).

3.3. Relaxation

Table 3 shows the average spin–spin relaxation time T_{2m} (Eq. (2)) and the relaxation spectra (A_i(%), T_{2i}) for the dispersed phase (aqueous phase), the continuous phase (organic phase), the just prepared W/O emulsions F1-F4 and the corresponding 24 h aged emulsions (after reconstitution) (20 °C).

All aqueous phases are characterised by much smaller relaxation time T_{2m} than that of the continuous organic phase, an essential aspect for the determination of the particle size distribution by LF NMR. Results presented in Table 3 show that the freshly prepared emulsion and the 24

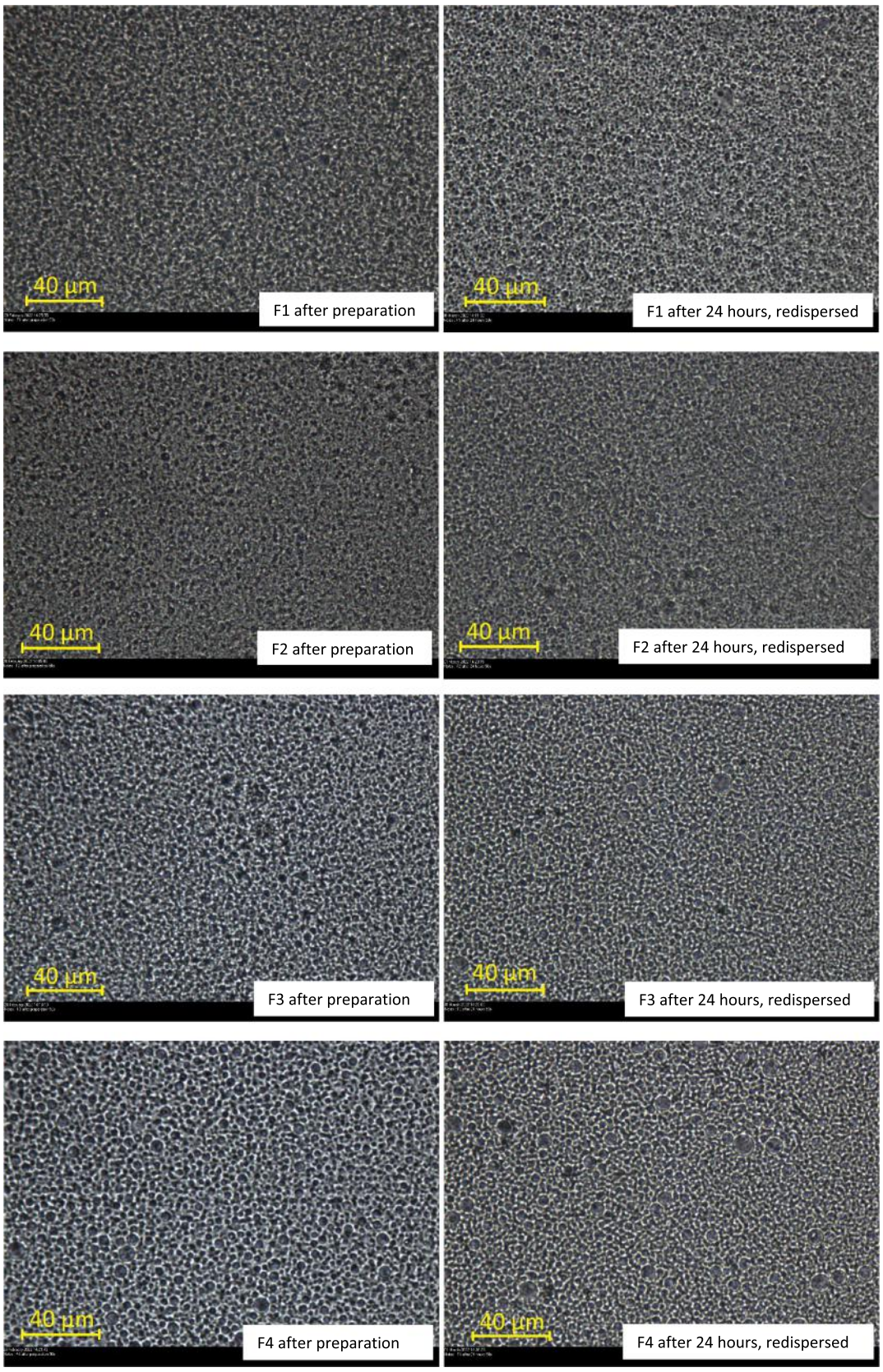

Fig. 1. Microscopic images of DCM-based W/O emulsions F1 -F4 immediately after preparation (left panels) and redispersed emulsions after 24 h (right panels). Magnification 50 ×.

Table 2
DLS characterization of emulsions F1-F4. *Start* indicates the just prepared emulsion while *After* indicates a just shaked emulsion after 24 h of storage at room temperature.

		F1		F2		F3		F4	
		Start	After 24 h	Start	After 24 h	Start	After 24 h	Start	After 24 h
Z-average (nm)	Mean	1589	1534	1430	1509	2136	2134	1997	2118
	Standard deviation	60.74	35.78	39.31	27.63	82.1	156.6	239.7	174.5
	Minimum	1519	1494	1385	1479	2044	1968	1727	1932
	Maximum	1633	1562	1459	1533	2203	2279	2183	2278
Polydispersity index	Mean	0.1889	0.1599	0.3192	0.3285	0.4666	0.1694	0.06678	0.1367
	Standard deviation	0.07863	0.05288	0.05346	0.05465	0.5007	0.1305	0.0495	0.09334
	Minimum	0.1	0.09932	0.2615	0.2949	0.006844	0.02718	0.01678	0.02915
	Maximum	0.2494	0.197	0.367	0.3916	1	0.2836	0.1158	0.1969

Table 3
Relaxation behaviour of emulsions F1-F4. T_{2i} represent the different relaxation times while A_i (%) are the corresponding percentual fractions. F1-F4 are the four different formulations considered.

	T_{2m} (ms)	T_{21} (ms)	A_1 (%)	T_{22} (ms)	A_2 (%)	T_{23} (ms)	A_3 (%)	T_{24} (ms)	A_4 (%)
F1									
Aqueous phase	***804***	*804*	*100*						
Organic phase	***3513***	*3513*	*100*						
W/O emulsion, day 0	**1757**	2973	57	476	8	96	35		
W/O emulsion, after 24 h	**1838**	2738	64	1003	7	318	6	44	23
F2									
Aqueous phase	**359**	384	90	125	10				
Organic phase	**3513**	3513	100						
W/O emulsion, day 0	**1600**	2800	55	497	7	109	19	48	19
W/O emulsion, after 24 h	**1876**	2791	65	466	10	54	25		
F3									
Aqueous phase	**65**	73	63	49	33	15	4		
Organic phase	**3168**	3585	86	565	14				
W/O emulsion, day 0	**2693**	3814	68	614	9	106	22		
W/O emulsion, after 24 h	**2445**	3497	66	641	17	133	17		
F4									
Aqueous phase	**65**	73	63	49	33	15	4		
Organic phase	**3513**	3513	100						
W/O emulsion, day 0	**2911**	3565	80	380	13	109	7		
W/O emulsion, after 24 h	**2879**	3661	76	508	14	110	10		
W/O emulsion, after 24 h, not reconstituted	**3384**	4341	55	3025	32	292	13		

h aged reconstituted emulsion have not only similar T_{2m}, but also a similar relaxation spectrum. This means that shaking is sufficient to restore the original structure of the emulsion. In contrast, a completely different relaxation spectrum occurs when shaking is not used (as observed with the F4 emulsion), reflecting a completely different microstructure due to the segregation of the emulsion. The absence of a solute (other than vancomycin hydrochloride) in the aqueous phase of F1 results in the highest T_{2m} value among those competing to the four aqueous phases considered. The addition of P407 (F2) or chitosan (F3, F4) leads to a decrease in T_{2m} in the aqueous phase as well as the occurrence of more than one relaxation time T_{2i}, resulting in solutions that are not completely homogeneous (only one relaxation time should occur in a completely homogeneous solution).

This effect is more pronounced in aqueous phases containing chitosan due to the effect that its polymer chains exert on the relaxation behaviour of the water molecules in their vicinity. Moreover, the effect of P407 in reducing T_{2m} in the aqueous phase is less pronounced than that of chitosan, which can be justified by the different chemical and physical properties of the P407 micelles compared to the chitosan chains (in solution). In the organic phase, it can be seen that the addition of a small amount of sorbitan monooleate (F3) leads to a small reduction in T_{2m} and the occurrence of two relaxation times, indicating the formation of a solution that is not completely homogeneous. Since the freshly prepared and the 24 h aged emulsions generally have similar T_{2m} (the worst situation, F2, implies a T_{2m} deviation of 17.25 %) and similar relaxation spectra (A_i(%) - T_{2i}), it can be concluded that shaking is sufficient to restore the original emulsion structure.

Although it is always very difficult to speculate on the spatial organisation of such complex structures based on the relaxation spectra (A_i(%), T_{2i}), Table 3 shows an interesting aspect. Since the percentage mass fraction of the aqueous phase is about 9.1 % (5/55), one can speculate that the fingerprint of the aqueous phase in the emulsion is represented by the underlined components of the relaxation spectra (Table 3). This assumption is true in the case of F1, F2 and F4, since the underlined component is about 9.1 % and the corresponding relaxation time T_{2i} is not so far from the relaxation time of the aqueous phase. In the case of F3, the percentage is about double 9.1 % and we should refer to the effect of the presence of sorbitan monooleate in the organic phase. The presence of very similar proportions of underline in all freshly prepared and 24 h aged W/O emulsions ensures the reconstitution of the emulsion structure after shaking. However, emulsions F3 and F4 show the highest structural reproducibility when comparing the freshly prepared and the 24 h aged reconstituted sample, as the number of relaxation times T_{2i} is the same and their values are very similar. This evidence could be explained by the different stabilisers used to prepare the four emulsions, so that the reason why emulsions F3 and F4 showed the greatest tendency to recover their original structure when shaken after one day of rest should be due to the presence of chitosan. Indeed,

chitosan, a hydrophilic polymer, forms a network in the inner water droplets that stabilises the system (McClements and Dickinson, 1996; Zhu et al., 2019).

All these considerations lead to the conclusion that, LF NMR, allowing the analysis of the magnetic relaxation fingerprint (A_i, T_{2i}) of the emulsion, is a suitable tool for comparing the structures of the different emulsions.

3.4. Diffusion and droplet size distribution

As Fig. 2 suggests that R becomes almost constant for $\Delta \geq 20$ ms, it was decided to choose $\Delta_{min} = 20$ ms. The self-diffusion coefficients (D) for the four aqueous phases at 20 °C are: $D_{F1} = 1.445 \times 10^{-9}$ m^2/s, $D_{F2} = 1.030 \times 10^{-9}$ m^2/s, $D_{F3} = 1.509 \times 10^{-9}$ m^2/s and $D_{F4} = 1.476 \times 10^{-9}$ m^2/s. It is interesting to note that F1, F3 and F4 have a very similar value of the self-diffusion coefficient, while F2 is characterised by a smaller D value. The presence of P407 in F2 is reflected in a smaller reduction in the aqueous phase T_{2m} (55 %) and in a greater reduction in mobility (30 %) compared to chitosan. The enormous reduction (92 %) in the average relaxation time of the aqueous phase (see T_{2m} in Table 4) by chitosan (F3, F4) is not reflected in a corresponding reduction in the mobility of the water molecules.

This is undoubtedly due to the different way in which chitosan and P407 interact with the water molecules, resulting in a different organisation of the water molecules around the two solutes. Based on the choice of $\Delta_{min} = 20$ ms and the measurement of the self-diffusion coefficient of water molecules in the aqueous phase, droplet size distribution of the four formulations was determined, as shown in Table 4.

Fig. 3 shows the (volume) droplet size distribution of the four formulations. It confirms the assumption that the tested emulsions mainly contain droplets with a diameter of about 1 μm to 10 μm. Indeed, relying on what is shown in Fig. 4, it is possible verifying that about 65 % of the particles fall in the diameter range 1–10 μm for all formulations (volume distribution). Emulsion F4 exhibits narrower droplet size distribution than the other formulations. This indicates that the higher the viscosity of the inner phase (due to the presence of chitosan in the inner phase), the more difficult it is for the emulsification process to obtain a wide range of microparticles (Wu et al., 2014).

The addition of sorbitan monooleate to the organic phase of the formulation with chitosan in the dispersed phase (F3) led to a broader droplet size distribution. However, it did not significantly reduce the droplet size, when compared to F4. This observation is not consistent with previous studies in which the presence of sorbitan monooleate reduced droplet size. However, the latter effect is dependent on the surfactant concentration (Ray et al., 2015).

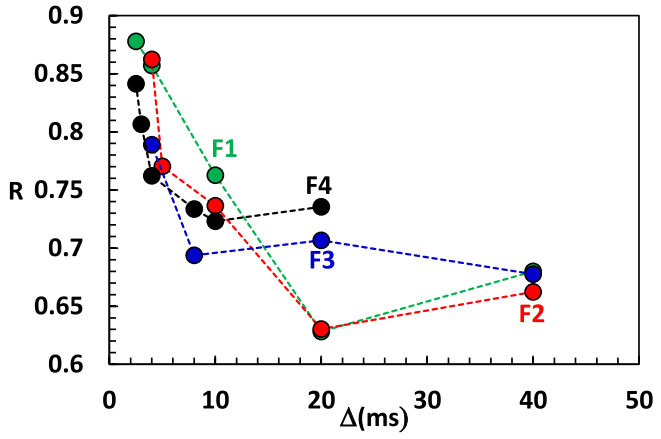

Fig. 2. R-values dependence on Δ for $\delta = 1$ ms referring to the four formulations considered (20 °C). R indicates the ratio between the LF NMR signal intensity with and without the application of two opposite magnetic field gradients of duration δand detached by a time interval equal to Δ.

Table 4
Parameters of the droplets size distribution referring to the freshly prepared emulsions.

	d_{50} (volume) (μm)	d_{50} (number) (μm)	σ (-)
F1	9.0 ± 0.90	2.50 ± 0.50	0.660 ± 0.050
F2	8.8 ± 0.50	4.60 ± 0.60	0.460 ± 0.040
F3	9.0 ± 0.50	3.80 ± 0.50	0.530 ± 0.030
F4	8.2 ± 0.04	4.36 ± 0.05	0.459 ± 0.004

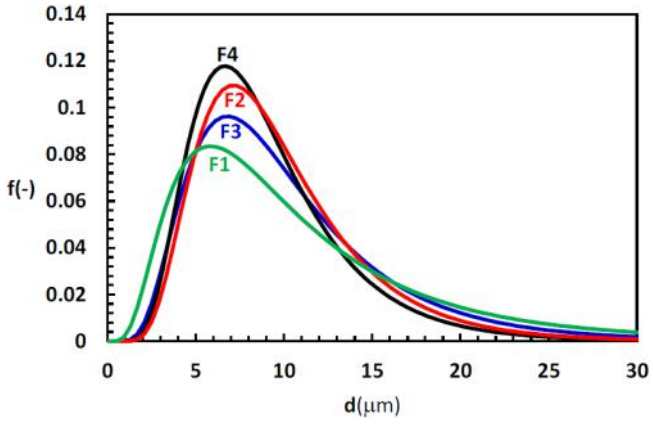

Fig. 3. (Volume) droplets size distribution of freshly prepared emulsions F1 – F4 (20 °C; d represents droplets diameter).

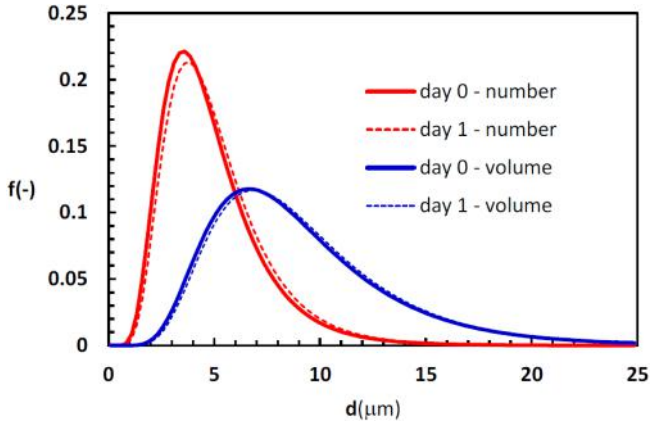

Fig. 4. Number (red lines) and volume (blue lines) droplet size (d - diameter) distribution of freshly prepared (solid red and blue lines) and the 24 h aged emulsion F4 after reconstitution (dashed red and blue lines). (For interpretation of the references to colour in this figure legend, the reader is referred to the web version of this article.)

Fig. 4 shows the number and volume distribution of the freshly prepared and the 24 h aged, reconstituted emulsion F4. It can be seen that the variations in both, number (red lines) and volume distribution, (blue lines) are negligible. Interestingly, a reasonably good agreement between the number droplets size distribution shown in Fig. 4 and the mean particle size determined by DLS (Table 2) can be seen. The droplet size distribution of the 24 h aged emulsions F1, F2 and F3 after reconstitution was not analysed.

However, results in Table 3 suggests that the droplet size distribution of the fresh and the 24 h aged reconstituted emulsion should not differ too much, as the relaxation spectra (A_i(%) - T_{2i}) and the average relaxation time (T_{2m}) of the different formulations are quite similar.

3.5. Rheological characterization

The rheology of bulk liquids plays an important role in controlling droplet size distribution in the spray drying process.

Non-Newtonian fluids, such as emulsions, often exhibit shear-thinning behaviour where viscosity decreases with increasing shear rate. If measurements are performed to predict or model atomisation processes or to check batches of feedstock prior to spray drying, it is essential that they are made at increased shear rates that are more relevant to the process. On the other hand, viscosity measurements at lower shear rates provide information on the long-term stability of the emulsion.

Fig. 5 and Fig. 6 show the flow curves in terms of viscosity (η) vs shear rate ($\dot{\gamma}$) and shear stress (τ_{rz}), respectively, for the four formulations.

As expected, these emulsions show non-Newtonian behaviour characterised by a decrease in η with $\dot{\gamma}$ or τ_{rz} (shear thinning). In addition, the inspection of Figs. 5 and 6 reveals that the R-P Cross model (eq.(5)) provides a better description of the flow than the power law (eq.(4)). As the four emulsions share similar droplet size distributions and volume fraction of the dispersed phase, characteristics that could strongly influence the flow curve, the differences between the flow curves should be attributed to the different viscosity behaviour of the organic and aqueous phases that make up each emulsion. Indeed, the high zero shear viscosity of F4, which is 2–3 orders of magnitude higher than that of the other formulations, could be be explained by the presence of chitosan, a hydrophilic polymer,that can increase in the inner water droplets viscosity. As a matter of fact, a higher zero shear viscosity indicates that the movement of droplets through the continuous phase is reduced, making coalescence less likely and increasing the long term stability of the emulsion at rest.

4. Determination of flow conditions

Flow conditions (1) refer to a flow rate ≈ 1.5 mL/min in a segment of flexible tubing that passes through the peristaltic pump of the spray dryer with inner diameter 1.02 mm and length 41 cm.

The power law model and the definition of the Reynolds number for non-Newtonian fluids:

$$R_e = \frac{v_{av}^{2-n} D^n \rho}{\eta_0 8^{n-1}} \tag{16}$$

where v_{av} is the average velocity (=$Q/\pi R_p^2$), ρ is fluid density, D is tube diameter and η_0 derives from eq.(4) best fitting to Fig. 5 experimental data, allow to evaluate the flow conditions inside the tube. Assuming $\rho = 1000$ kg/m^3 (water density) and knowing that the average velocity is equal to 3.06×10^{-2} m/s, Reynolds number turns out to be equal to 11.3, 10.5, 14.7 and 7.8 for formulations 1, 2, 3 and 4, respectively, i.e. much smaller than 2100 that indicates the limit of the laminar flow conditions.Fig. 7 makes clear that F1 and F4 show similar velocity and shear rate profiles inside the tube. Similarly, F2 and F3 share equivalent velocity and shear rate profile. This is reasonable since F1 and F4 are characterized by the highest values of the zero shear viscosity η_0 while F2 and F3 share the lowest η_0 values (see Fig. 5 and Fig. 6).

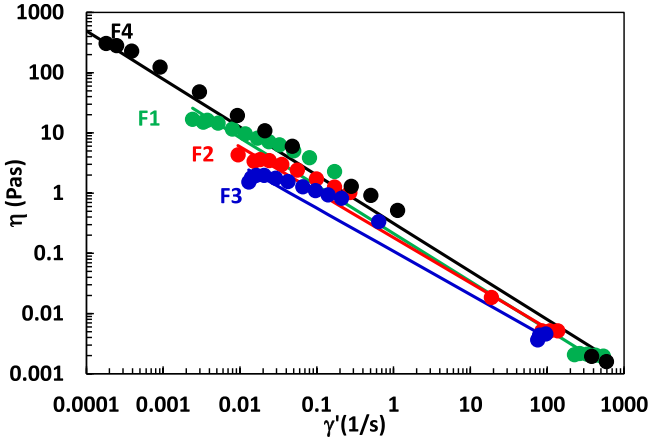

Fig. 5. Flow curve. Viscosity (η) reduction versus shear rate ($\dot{\gamma}$) referring to the four formulations considered. Continuous lines represent the best fitting of the power law (eq. (4)). Fitting parameters read: F1 (n = 0.205, η_0 = 0.214 Pa s^n), F2 (n = 0.247, η_0 = 0.183 Pa s^n), F3 (n = 0.282, η_0 = 0.108 Pa s^n), F4 (n = 0.201, η_0 = 0.315 Pa s^n).

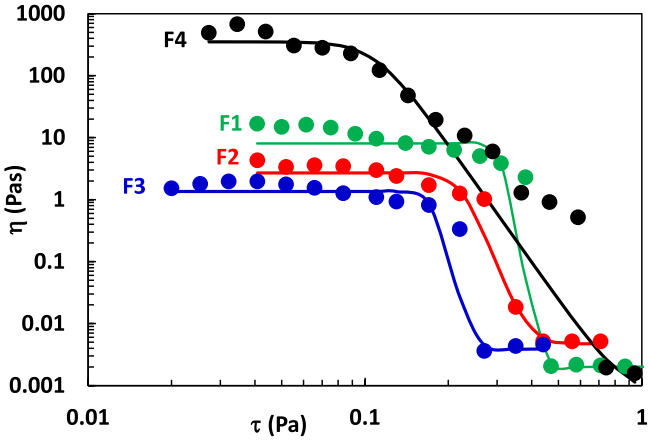

Fig. 6. Flow curve. Viscosity (η) reduction versus shear stress (τ) referring to the four formulations. Continuous lines represent the best fitting of the R-P Cross model (eq. (5)). Fitting parameters read: F1 (n = –23.2, η_0 = 8.1 Pa s, η_∞ = 20 × 10^{-4} Pa s, τ_s = 0.310 Pa), F2 (n = -10.3, η_0 = 2.7 Pa s, η_∞ = 47 × 10^{-4} Pa s, τ_s = 0.22 Pa), F3 (n = -17, η_0 = 1.35 Pa s, η_∞ = 39 × 10^{-4} Pa s, τ_s = 0.17 Pa), F4 (n = -5.3, η_0 = 351.7 Pa s, η_∞ = 7 × 10^{-4} Pa s, τ_s = 0.109 Pa).

Flow condition (2) refer to a flow rate ≈ 1.5 mL/min in the non-flexible tubing, before the pump and after the pump, characterised by an inner diameter of 1.8 mm and a length of 115 cm. Assuming $\rho = 1000$ kg/m^3 (water density) and the average velocity is 9.8×10^{-3} m/s, the Reynolds number is 1.66, 1.66, 2.46 and 1.14 for formulations 1, 2, 3 and 4, respectively, i.e. much smaller than 2100 indicating the limit of laminar flow conditions.

Fig. 8 makes it clear that all formulations give similar velocity and shear rate profiles when R_e is small. Obviously, they all show the typical non-Newtonian shape characterised by a flat trend in the inner part of the tube followed by an abrupt decrease towards the wall. Flow condition (2) means a slightly lower shear stress at the tube wall (where it is maximum) (data not shown) and a significant reduction in the shear rate amplitude, which now ranges from zero (tube axis) to about −100 s^{-1} at the tube wall. Flow condition (1) is thus more severe than flow condition (2), which is due to the different internal diameters of the two types of tube used. The flow conditions described, which are assigned to a feed tube of a laboratory-scale spray dryer, represent the worst case in terms of shear stress. Scaling up the process requires the use of larger diameter tubes that should lead to a reduction in the Reynolds number with a positive effect on the stability of the emulsions. Anyway, this analysis allows the calculation of the Reynolds number and the determination of the shear rate/shear stress for each type of tube, thus providing a useful tool for scaling up the spray drying process of emulsions. Of course, in this analysis we have neglected what happens inside the peristaltic pump where, as assumed, the emulsion is subjected to a higher shear rate and shear stress.

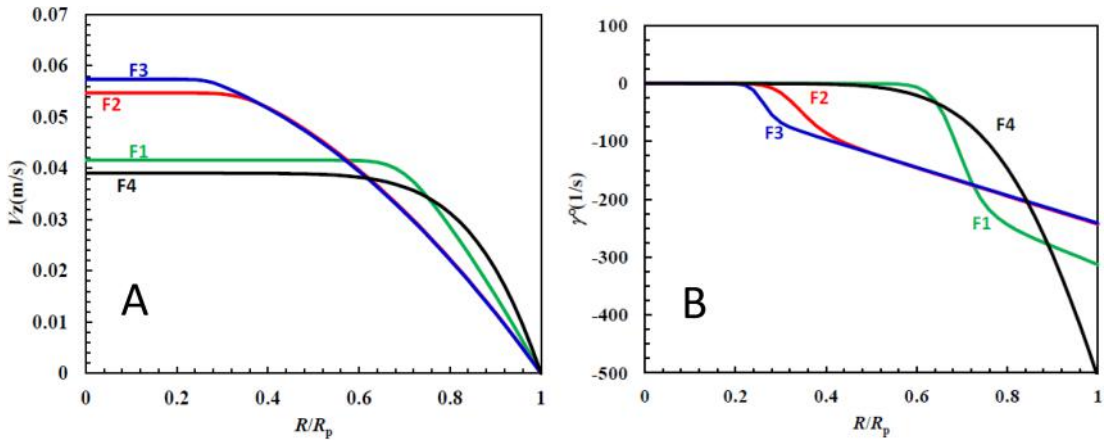

Fig. 7. Velocity (A) and shear rate (B) profile referring to the four formulations in Flow conditions (1) according to the R-P Cross model (eq. (5)). R_p is the tubing radius and R/R_p is the dimensionless radial position ($R/R_p = 1$ indicate tubing wall).

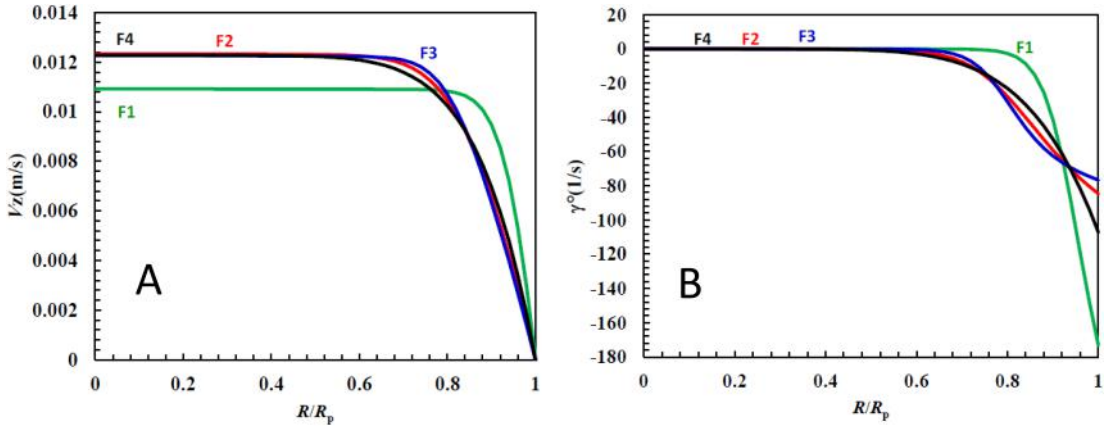

Fig. 8. Velocity (A) and shear rate (B) profile referring to the four formulations in Flow condition (2) according to R-P Cross model (eq. (5)). R_p is the tubing radius and R/R_p is the dimensionless radial position ($R/R_p = 1$ indicate tubing wall).

5. Conclusion

The combined use of different techniques, namely visual observation, microscopic images, DLS, low-field NMR and rheology allowed us to obtain useful information about the microstructure and stability of the PLGA/DCM-based emulsions studied. Low-field NMR not only allowed us to determine the droplet size distribution, which was also confirmed by the microscope images, but also provided information on the volume fraction (A_i) competing with the aqueous and organic phases pervading the different emulsions, as well as on their magnetic relaxation time (T_{2i}), i.e. the emulsion finger print. The analysis of the fingerprints of the freshly prepared emulsions and the emulsions aged for one day confirmed that a simple shaking was sufficient to restore the original structure of the emulsions. Thus, LF NMR proved to be a suitable tool to compare the structures of the different emulsions.

On the other hand, rheology plays a fundamental role in determining one of the most important properties of a fluid, namely the dependence of viscosity on flow conditions (shear rate/shear stress), the well-known flow curve. Not only can the flow curve be considered as a rheological fingerprint of a fluid that allows comparison between different emulsions, but its knowledge is also necessary to determine the flow conditions (shear rate/shear stress) to which the fluid is subjected when flowing in a tube. These conditions can in fact strongly influence the structure of the emulsion, which affects the properties of the final dry product. It is well known that knowledge of the flow curve is fundamental to realise a correct scale-up from laboratory to production scale. Based on this analysis, we found that the four emulsions have the same non-Newtonian shear thinning behaviour, even though they differ mainly in terms of the value of zero shear viscosity. Finally, knowledge of the flow curves proved that laminar flow occurred in all our connecting tubes. Using appropriate mathematical models capable of describing the experimental flow curves, we were also able to solve the momentum balance to obtain the shear rate and shear stress profiles of the flowing fluid and, of course, the velocity profile of the fluid. In this way, we were able to structurally characterise the emulsions at rest and the flow conditions in the different feed tubes of the spray dryer.

Further studies on emulsion drying and characterisation of the obtained vancomicyn-loaded PLGA microparticles should provide information on the relationship between stability, microstructure and flow behaviour of the initial emulsion and the quality of the final product.

CRediT authorship contribution statement

Ana Jurić Simčić: Conceptualization, Methodology, Validation, Investigation, Formal analysis, Data curation, Writing – original draft. **Michela Abrami:** Conceptualization, Methodology, Validation, Investigation, Formal analysis, Data curation, Writing – original draft. **Iva Erak:** Investigation. **Iva Paladin:** Investigation. **Biserka Cetina Čižmek:** Writing – review & editing, Supervision. **Anita Hafner:** Writing – review & editing, Supervision. **Mario Grassi:** Writing – review & editing, Supervision. **Jelena Filipović-Grčić:** Writing – review & editing, Supervision, Project administration, Funding acquisition.

Declaration of Competing Interest

The authors declare that they have no known competing financial interests or personal relationships that could have appeared to influence the work reported in this paper.

Data availability

Data will be made available on request.

Acknowledgements

This work was funded by R&D, PLIVA Croatia Ltd, TEVA Group Member, Croatia grant 644-01/15-01/01, Modelling of the Pharmaceutical Spray-Drying Process of the Emulsions in Laboratory and Pilot Scale.

References

Behrend, O., Ax, K., Schubert, H., 2000. Influence of continuous phase viscosity on emulsification by ultrasound. Ultrasonic Sonochemistry 7, 77–85.

Billon, A., Chabaud, L., Gouyette, A., Bouler, J.M., Merle, C., 2005. Vancomycin biodegradable poly(lactide-co glycolide) microparticles for bone implantation. Influence of the formulation parameters on the size, morphology, drug loading and in vitro release. J Microencapsul. 22 (8), 841–852.

Bird, R.B., Stewart, W.E., Lightfoot, E.N., Klingerberg, D.J. 2015. Introductory Transport Phenomena, chapter 2. Wiley, Danvers, USA.

Chui, M., Phillips, R., 1995. Measurement of the porous microstructure of hydrogels by nuclear magnetic resonance. J Colloid Interface Sci. 174, 336–344.

De Rosa, G., Iommelli, R., La Rotonda, M.I., Miro, A., Quaglia, F., 2000. Influence of the co-encapsulation of different non-ionic surfactants on the properties of PLGA insulin-loaded microspheres. J Control Release 69 (2), 283–295.

Dinarvand, R., Moghadam, S.H., Sheikhi, A., Atyabi, F., 2005. Effect of surfactant HLB and different formulation variables on the properties of poly-D, L-lactide microspheres of naltrexone prepared by double emulsion technique. J Microencapsul. 22 (2), 139–151.

Draper, N.R., Smith, H. 1966. Applied Regression Analysis. John Wiley & Sons Inc, New York.

Guido, S., 2011. Shear-induced droplet deformation: Effects of confined geometry and viscoelasticity. Curr. Opin. Colloid Interface Sci. 16, 61–70.

Guido, S., Preziosi, V., 2010. Droplet deformation under confined Poiseuille flow. Adv. Colloid Interface Sci. 161, 89–101.

Janssen, J.M.H., Meijer, H.E.H., 1993. Droplet breakup mechanisms: Stepwise equilibrium versus transient dispersion. J. Rheol. 37, 597–608.

Kang, F., Jiang, G., Hinderliter, A., DeLuca, P.P., Singh, J., 2002. Lysozyme Stability in Primary Emulsion for PLGA Microsphere Preparation: Effect of Recovery Methods and Stabilizing Excipients. Pharm Res. 19, 629–633.

Klinkesorn, U., 2013. The Role of Chitosan in Emulsion Formation and Stabilization. Food Rev. Intl. 29 (4), 371–393.

Liu, B., Dong, Q., Wang, M., Shi, L., Wu, Y., Yu, X., Shi, Y., Shan, Y., Jiang, C., Zhang, X., Gu, T., Chen, Y., Kong, W., 2010. Preparation, characterization, and pharmacodynamics of exenatide-loaded poly(DL-lactic-co glycolic acid) microspheres. Chem Pharm Bull 58 (11), 1474–1479.

McClements, D.J., Dickinson, E., 1996. Advances in Food Colloids. Glasgow, Chapman and Hall.

Meiboom, S., Gill, D., 1958. Modified Spin-Echo Method for Measuring Nuclear Relaxation Times. Rev. Sci. Instrum. 29, 688–691.

Mezger, T.G. 2015. Applied Rheology with Joe Flow on Rheology Road. Anton Paar GmbH, Graz, Austria.

Mohammed, A., Okoye, S.I., Salisu, J., 2016. Effect of Dispersed Phase Viscosity on Stability of Emulsions Produced by a Rotor Stator Homogenizer. International Journal of Sciences: Basic and Applied Research 25 (2), 256–267.

Panigrahi, D., Sahu, P.K., Swain, S., Verma, R.K., 2021. Quality by design prospects of pharmaceuticals application of double emulsion method for PLGA loaded nanoparticles. SN Appl. Sci. 3, 638.

Porfirio, T., Galindo-Rosale,s F.J., Campo-Deaño, L., Vicente, J., Semião, V. 2021. Rheological characterization of polymeric solutions used in spray drying process. Eur. J. Pharmaceut. Sci., 158, 928-987.

Ray, S., Mishra, A., Mandal, T.K., Sa, B., Chakraborty, J., 2015. Optimization of the process parameters for the fabrication of a polymer coated layered double hydroxide-methotrexate nanohybrid for the possible treatment of osteosarcoma. RSC Adv. 5, 102574–102592.

Shah, S.R., Henslee, A.M., Spicer, P.P., Yokota, S., Petrichenko, S., Allahabadi, S., Bennet, G.N., Wong, M.E., Kasper, F.K., Mikos, A.G., 2014. Effects of antibiotic physicochemical properties on their release kinetics from biodegradable polymer microparticles. Pharm Res. 31 (12), 3379–3389.

Sjöblom, J., Mhatre, S., Simon, S., Skartlien, R., Sørland, G., 2021. Emulsions in external electric fields. Adv Colloid Interface Sci. 294, 102455.

Soomherun, N., Kreua-Ongarjnukool, N., Chumnanvej, S., Thumsing, S., 2017. Encapsulation of Nicardipine Hydrochloride and Release from Biodegradable Poly (D, L-lactic-co-glycolic acid) Microparticles by Double Emulsion Process: Effect of Emulsion Stability and Different Parameters on Drug Entrapment. Int J Biomater. 2017, 1–13.

Stilbs, P., 1987. Fourier transform pulsed-gradient spin-echo studies of molecular diffusion. Progress in NMR Spectroscopy 19, 1–45.

Tadros, T.F. 2016. Emulsions: Formation, Stability, Industrial Applications. Berlin, Boston, De Gruyter.

Taghipour, B., Yakhchali, M., Haririan, I., Tamaddon, A.M., Samani, S.M., 2014. The effects of technical and compositional variables on the size and release profile of bovine serum albumin from PLGA based particulate systems. Res Pharm Sci. 9 (6), 407–420.

Tolstoguzov, V.B., Mzhel'sky, A.I., Gulov, V.Y., 1974. Deformation of emulsion droplets in flow. *Colloid Polym. Sci. Kolloid-Zeitschrift Zeitschrift für Polym. 252*, 124–132.

Wan, F., Yang, M., 2016. Design of PLGA-based depot delivery systems for biopharmaceuticals prepared by spray drying. Int J Pharm. 498 (1–2), 82–95.

Wu, G., Chen, L., Li, H., Deng, C.L., Chen, X.F. 2014. Comparing microspheres with different internal phase of polyelectrolyte as local drug delivery system for bone tuberculosis therapy. *Biomed Res Int., 2014*, 297808.

Ye, M., Kim, S., Park, K., 2010. Issues in long-term protein delivery using biodegradable microparticles. J Control Release 146 (2), 241–260.

Zhang, M., Yang, B., Liu, W., Li, S., 2017. Influence of hydroxypropyl methylcellulose, methylcellulose, gelatin, poloxamer 407 and poloxamer 188 on the formation and stability of soybean oil-in-water emulsions. Asian J. Pharm. Sci. 12 (6), 521–531.

Zhu, Q., Pan, Y., Jia, X., Li, J., Zhang, M., Yin, L., 2019. Review on the Stability Mechanism and Application of Water in-Oil Emulsions Encapsulating Various Additives. Compr. Rev. Food Sci. Food Saf. 18 (6), 1660–1675.